Original Research Article

Fractional Order Modeling of 1,2,3 DOF Robot Dynamic

Israel Cerón-Morales

Instituto Tecnológico Superior de Poza Rica Ingeniería Electrónica, CP 93230, pozarika, Veracruz, Mexico

ABSTRACT

The fractional order modeling method of robot dynamics with one, two and three degrees of freedom is introduced. The stability of the fractional order model is proved by using the second-order Lyapunov method. A basic physical parameter is considered, that is, the inertial mass of the connecting rod. Freecad software is used for mechanical design. The dynamic models of 2-DOF and 3-DOF robots are established, and their motion trajectories are given in plane (x, y) and space (x, y, z) respectively. The model is programmed on the development card based on microcontroller. The advantage of the development card lies in its peripheral output, because it has two analog output channels, which are sent to the oscilloscope. The results are consistent with the proposed model.

Keywords: Machine Translation; Deep Learning; Neural Machine Translation; Urdu Language; Chinese Language

*CORRESPONDING AUTHOR

Israel Cerón-Morales
E-mail: israel.ceron@itspozarica.edu.mx

1. Introduction

Mathematical model is the approximate value of physical system behavior. In the existing mathematical tools, fractional-order calculus (FOC) has interesting characteristics compared with integer order calculation. In the subject of system dynamics modeling, FOC has better approximation than integer order calculation. For example, FOC is applied to the modeling of diver system. The circuit dynamics model based on integer order differential equation shows the difference between the experimental data and the data generated by the model. The widely studied circuit is a circuit composed of resistance and capacitance in series. Due to the difference between integer order model data and experimental data, the model of the circuit is questioned. Gómez-Aguilar[1] proposed the fractional order model of RC circuit. The error of the data of the fractional order model is much smaller than that of the integer order model. Goodvine[2] introduced the application of FOC in the study of welding process dynamics. Tejado[3] applied FOC to the study of human arm, and Rosario[4] used FOC on the axis of robot arm. Shalaby[5] introduced an inverted pendulum into the FOC model. Zhang[6] introduced FOC when estimating the CARC state of supercapacitors. Shi et al.[7] proved that FOC based control can suppress interference, and Ceron-Morales[8] realizes the control of solar concentrator through FOC.

For robots that can be modeled with various technologies[9], one of the widely used robot modeling equations is Euler-Lagrange equation, and the result is an integer order differential equation system. The proposed fractional order model must first meet the stability conditions. If the fractional order model meets the stability requirements, it can be simulated and applied to practical purposes. Therefore, the stability pro-

of using Lyapunov's second criterion is given.

It is difficult to apply fractional order modeling to the actual situation[10]. Therefore, this paper uses the development card to realize the fractional order modeling of one, two and three degree of freedom (DOF) robots, and reports the implementation of using multiple microcontrollers. Like the work of Flores-Ordeñana et al.[11], in which STM32 card is used for its built-in advantages[12,13].

This work is limited to showing the simulation results realized on the STM32L476 development card, because building a robot with the simplest design parameters requires financial investment, which cannot be realized at present.

2. Development

The robot connecting rod is a mechanical part, which has mechanical properties that must be determined digitally. As shown in the **Figure 1**, you can see a connecting rod designed in a free software called FreeCAD.

The mechanical parameters required for dynamic simulation are mass moment of inertia (also known as moment of inertia) and center of mass position. The parts must be solid materials and their bulk mass density must be known data (ρ). **Table 1** divides the connecting rod into four basic geometric figures and specifies the equations for calculating mass moment of inertia and center of mass.

The parallel axis theorem is used to calculate the moment of inertia mass of the combined graph. When calculating the moment of inertia mass of the complete graph, the moment of inertia of the hollow graph is neg-

ative. Use the equations in **Table 1** to design the connecting rod parameters, and take into account the materials with known mass bulk density. Then calculate the mass of mechanical components, and design the robot mechanism according to these known numerical values. The simplest is the single connecting rod mechanically coupled to the motor[14]. Taking the mechanism as the starting point, the dynamic model of the mechanism is established.

Considering the single degree of freedom manipulator (1DOF) diagram shown in **Figure 2**, parameters such as mass, length and moment of inertia are observed. These mechanical parameters and simulation values are shown in **Table 2**.

The first-order integer mathematical model is obtained by using Euler-Lagrange equation. The obtained dynamic model is (1):

$$\tau = (ml^2 + I)\ddot{q} + b\dot{q} + mgl_c\,sen(q) \tag{1}$$

The goal is to position the linkage at the desired (q_d) angle. (1) is written in the form of state variables (2) and (3):

$$\tilde{q} = q_d - q \tag{2}$$

$$\dot{q} = \frac{dq}{dt} \tag{3}$$

According to the state variables, the dynamic system is shown in (4):

$$\frac{d}{dt}\begin{bmatrix} \tilde{q} \\ \dot{q} \end{bmatrix} = \left[\left(ml^2 + I\right)^{-1}\left(\tau - bq - mgl_c\,sen(q)\right) \right] \tag{4}$$
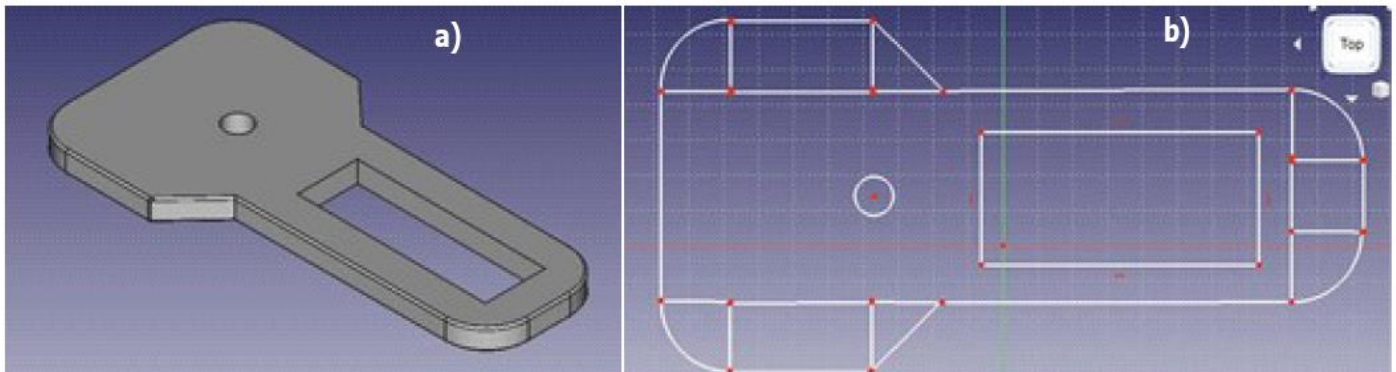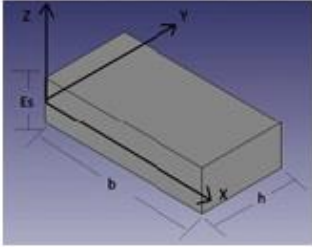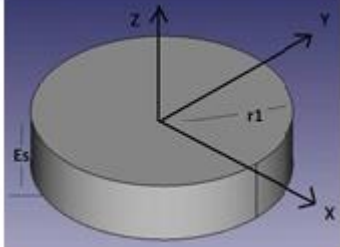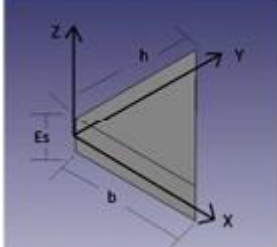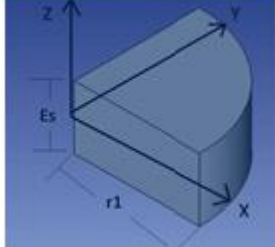

Figure 1. (a) Connecting rod design in FreeCAD; (b) dividing the connecting rod plane into basic geometric figures.

Table 1. An equation for calculating the basic parameters of the simple geometry constituting the robot connecting rod

Rectangular	Circular	Triangular	Bend

Mass moment of inertia

$(\rho \cdot Es) \cdot \left[\dfrac{bh^3}{12} + \dfrac{b^3 h}{12} \right]$	$\dfrac{r_1^2}{2} \cdot \left(\rho Es \pi r_1^2 \right)$	$\left(\dfrac{4\rho Es}{3} \right) \left(\dfrac{bh}{2} \right) \left[h^2 + b^2 \right]$	$\dfrac{r_1^2}{8} \cdot \left(\rho Es \pi r_1^2 \right)$

Centroid

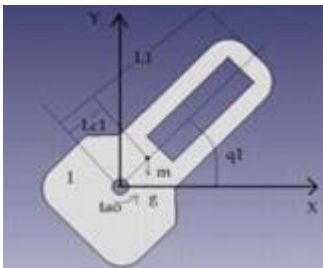|			
$\left(\dfrac{b}{2}, \dfrac{h}{2}, \dfrac{Es}{2} \right)$	$\left(0, 0, \dfrac{Es}{2} \right)$	$\left(\dfrac{b}{3}, \dfrac{h}{3}, \dfrac{Es}{2} \right)$	$\left(\dfrac{4r_1}{3\pi}, \dfrac{4r_1}{3\pi}, \dfrac{Es}{2} \right)$

If expressed by Laplace transform, we get (5).

$$\begin{bmatrix} s\tilde{q} \\ s\dot{q} \end{bmatrix} = \begin{bmatrix} -\dot{q}(s) \\ \left(ml^2 + I\right)^{-1}\left(\tau - b\dot{q}(s) - mgl_c \operatorname{sen}(q(s))\right) \end{bmatrix} \tag{5}$$

The integer derivative of the angular position function is represented by (6), and according to Krishna[2], the fractional derivative is (7).

$$L\left\{ \frac{dq(t)}{dt} \right\} = sq(s) \tag{6}$$

$$L\left\{ \frac{d^\mu q(t)}{dt^\alpha} \right\} = s^\mu q(s) \tag{7}$$

Figure 2. Connecting rod diagram of 1-DOF robot.

Equation (7) has an approximation of the quotient, which is the approximation of each continuous fraction in (8).

$$s^\mu q(s) \approx \frac{As+1}{s+A} \tag{8}$$

Table 2. Physical parameters of one degree of freedom manipulator

Parameter	Link 1	Value	Unit
quality	m	1	kg .
length	L	1	m
Center length quality	LC compa-ny	0.5	m
Moment of inertia	I	0.1	kg·m²
Viscous friction coefficient	b	0	N·m·s⁻¹
Torsion	τ	-	N
Angular position	q	-	Grade
angular velocity	$\dot{q}$	-	grade·s⁻¹
angular acceleration	$\ddot{q}$	-	grade·s⁻²

Conditions (9) and (10) must meet:

$$A = \frac{1+\mu}{1-\mu} \tag{9}$$

$$0 < \mu < 1 \tag{10}$$

Therefore, the fractional order approximation applied to model (5) is expressed as (11).

$$\begin{bmatrix} s^\mu \tilde{q} \\ s^\mu \dot{q} \end{bmatrix} = \begin{bmatrix} -\dot{q}(s) \\ \left(ml^2 + I\right)^{-1}\left(\tau - b\dot{q}(s) - mgl_c \operatorname{sen}(q(s))\right) \end{bmatrix} \tag{11}$$

(12) is obtained by replacing (8) in (11).

$$\begin{bmatrix} (As+1)\tilde{q} \\ (As+1)\dot{q} \end{bmatrix} = \begin{bmatrix} -(s+A)\dot{q}(s) \\ (ml^2+I)^{-1}(S+A)(\tau - b\dot{q}(s) - mgl_c \operatorname{sen}(q(s))) \end{bmatrix} \tag{12}$$

On this point, a proportional derivative control (15) plus gravity compensation in (13) is proposed. It is worth mentioning that PD control has neural network versions[12,16].

$$\tau = k_p\tilde{q} - k_v\dot{q}(s) + mgl_c \operatorname{sen}(q(s)) \tag{13}$$

By replacing (13) with (12) and executing the algebra shown, a compact equation can be obtained, with is supported by the variables shown in (14), (15), (16) and (17). Using the inverse Laplace transform, the result is (18).

$$A_{11} = \frac{A^3(ml^2+I) + A^2(k_v+b) + Ak_p}{A^2(ml^2+I) + A(k_v+b) + k_p} \tag{14}$$

$$A_{12} = \frac{1-A}{A} \tag{15}$$

$$A_{21} = \frac{k_p A(1-A)}{A^2(ml^2+I) + A(k_v+b) + k_p} \tag{16}$$

$$A_{22} = \frac{A^2(k_v+b) + A(ml^2+I+k_p)}{A^2(ml^2+I) + A(k_v+b) + k_p} \tag{17}$$

$$\frac{d}{dt}\begin{bmatrix} \tilde{q} \\ \dot{q} \end{bmatrix} = \begin{bmatrix} -A_{11}\tilde{q} + A_{12}\dot{q} \\ A_{21}\tilde{q} - A_{22}\dot{q} \end{bmatrix} \tag{18}$$

At this point, a candidate Lyapunov function (19) is proposed.

$$V(\tilde{q}, \dot{q}) = \frac{1}{2}k_1\tilde{q}^2 + \frac{1}{2}k_2\dot{q}^2 \tag{19}$$

It is deduced that the candidate Lyapunov function about time is (20).

$$\frac{d}{dt}V(\tilde{q}, \dot{q}) = k_1\tilde{q}\frac{d\tilde{q}}{dt} + k_2\dot{q}\frac{d\dot{q}}{dt} \tag{20}$$

(21) is obtained by substituting (18) into (20) and performing algebraic operations.

$$\frac{d}{dt}V(\tilde{q}, \dot{q}) = -CAk_1\tilde{q}^2 - CDk_2\dot{q}^2 - (A-1)(k_1 + k_2 k_p A^2)\tilde{q}\dot{q} \le 0 \tag{21}$$

The support (21) is considered to be (22).

$$\frac{d}{dt}V(\tilde{q}, \dot{q}) \le -\left((A_{11}k_1)^{\frac{1}{2}}\tilde{q} + (A_{22}k_2)^{\frac{1}{2}}\dot{q}\right)^2 \tag{22}$$

By developing the algebra shown in (22), result (23) completes the proof of Lyapunov stability of fractional order model.

$$-(A-1)(k_1 + k_2 k_p A^2)\tilde{q}\dot{q} \le$$
$$\le \sqrt{(k_1 A^3(ml^2+I) + k_1 A^2(k_v+b) + k_1 A^2 k_p)}$$
$$\sqrt{(k_2 A(A^2(k_v+b) + A(ml^2+I+k_p)))}\tilde{q}\dot{q} \tag{23}$$

The proof given shows that the equilibrium point of the new model is represented by (24).

$$\begin{bmatrix} \tilde{q} \\ \dot{q} \end{bmatrix} = \begin{bmatrix} 0 \\ 0 \end{bmatrix}\Bigg|_{t\to\infty} \tag{24}$$

The simulation results show that it is feasible to use the fractional order model for stability simulation, that is, the equations can be written in programming language, and the dynamic behavior of 1 DOF manipulator is simulated, (24) shows that the model has convergence. The simulation will be introduced later, and continue to introduce the modeling of 2 and 3 DOF robots. **Figure 3** shows a 2 DOF robot in which two connecting rods move on a plane.

The physical parameters of 2 DOF robot are shown in **Table 3**. The Euler-Lagrange model of robot 2 DOF is shown in (25)

$$\begin{bmatrix} \tau_1 \\ \tau_2 \end{bmatrix} = \begin{bmatrix} m_{11}(q) & m_{12}(q) \\ m_{21}(q) & m_{22}(q) \end{bmatrix}\begin{bmatrix} \ddot{q}_1 \\ \ddot{q}_2 \end{bmatrix} + \begin{bmatrix} b_1 & 0 \\ 0 & b_2 \end{bmatrix}\begin{bmatrix} \dot{q}_1 \\ \dot{q}_2 \end{bmatrix} +$$
$$+ \begin{bmatrix} c_{11}(q,\dot{q}) & c_{12}(q,\dot{q}) \\ c_{21}(q,\dot{q}) & c_{22}(q,\dot{q}) \end{bmatrix}\begin{bmatrix} \dot{q}_1 \\ \dot{q}_2 \end{bmatrix} + \begin{bmatrix} g_1(q) \\ g_2(q) \end{bmatrix} \tag{25}$$
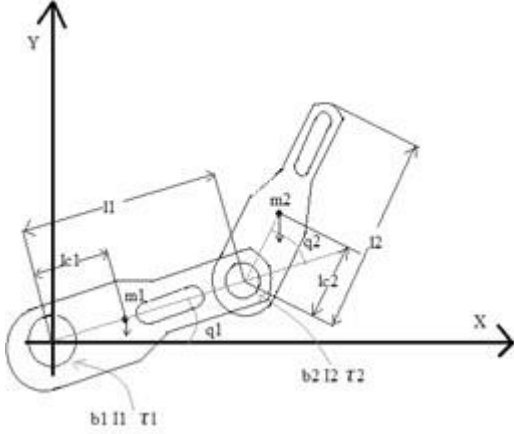
Figure 3. Schematic diagram of 2-DOF robot.

According to the physical parameters, the equation of the matrix element is shown between (26) and (35).

$$m_{11}(q) = m_1 lc_1^2 + m_2 lc_2^2 + I_1 + I_2 + 2m_2 l_1 lc_2 \cos(q_2) \quad (26)$$

$$m_{12}(q) = m_2 lc_2^2 + I_2 + m_2 l_1 lc_2 \cos(q_2) \quad (27)$$

$$m_{12}(q) = m_2 lc_2^2 + I_2 + m_2 l_1 lc_2 \cos(q_2) \quad (28)$$

Table 3. Physical parameters of 2-DOF manipulator

Parameter	Link 1	Link 2	Unit
quality	m_1	m_2	kg
	0.1	0.05	
length	L_1	L_2	m
	0.1	0.1	
Center length quality	Lc_1	Lc_2	m
	0.05	0.05	
Moment of inertia	I_1	I_2	kg·m²
	0.2	0.09	
friction coefficient	b1	b2	N·m·s⁻¹
Viscous	0.2	0.17	
Torsion	$\tau 1$	$\tau 2$	N
Angular position	q_1	q_2	Grade
angular velocity	$\dot{q}_1$	$\dot{q}_2$	grade·s⁻¹
angular acceleration	$\ddot{q}_1$	$\ddot{q}_2$	grade·s⁻²

$$m_{22}(q) = m_2 lc_2^2 + I_2 \quad (29)$$

Due to the symmetry of matrices and M (27) and (28), they are the same.

This C matrix, also known as the Coriolis matrix, represents terms (30) to (33). When an object moves to another rotating object, the Coriolis effect appears, which is why q_2 angle is an important dependency.

$$c_{11}(q) = -2m_2 l_1 lc_2 \dot{q}_2 \sin(q_2) n \quad (30)$$

$$c_{12}(q) = -m_2 l_1 lc_2 q_2 \sin(q_2) \quad (31)$$

$$c_{21}(q) = m_2 l_1 lc_2 q_1 \sin(q_2) \quad (32)$$

$$c_{22}(q) = 0 \quad (33)$$

The term due to gravity is given in (34) and (35).

$$g_1(q) = m_1 glc_1 \sin(q_1) + m_2 gl_1 \sin(q_1) + m_2 glc_2 \sin(q_1 + q_2) \quad (34)$$

$$g_2(q) = m_2 glc_2 \sin(q_1 + q_2) \quad (35)$$

The model is processed according to the state variables (36) to (39) and the substitution (40) in (25) is obtained.

$$q_1 = x_1 \quad (36)$$

$$q_2 = x_3 \quad (37)$$

$$\dot{q}_1 = x_2 = \dot{x}_1 \quad (38)$$

$$\dot{q}_2 = x_4 = \dot{x}_2 \quad (39)$$

To present a compact representation, (41) is used to simplify the matrix.

$$\begin{bmatrix} \dot{x}_1 \\ \dot{x}_3 \\ \dot{x}_2 \\ \dot{x}_4 \end{bmatrix} = \begin{bmatrix} \begin{bmatrix} 1 & 0 \\ 0 & 1 \end{bmatrix}\begin{bmatrix} x_2 \\ x_4 \end{bmatrix} \\ \begin{bmatrix} m_{11}^{-1}(x) & m_{12}^{-1}(x) \\ m_{21}^{-1}(x) & m_{22}^{-1}(x) \end{bmatrix}\begin{Bmatrix} f_1 \\ f_2 \end{Bmatrix} \end{bmatrix} \quad (40)$$

$$\begin{bmatrix} f_1 \\ f_2 \end{bmatrix} = \left\{ \begin{bmatrix} \tau_1 \\ \tau_2 \end{bmatrix} - \begin{bmatrix} c_{11}(x) & c_{12}(x) \\ c_{21}(x) & c_{22}(x) \end{bmatrix}\begin{bmatrix} x_3 \\ x_4 \end{bmatrix} - \begin{bmatrix} b_1 & 0 \\ 0 & b_2 \end{bmatrix}\begin{bmatrix} x_3 \\ x_4 \end{bmatrix} - \begin{bmatrix} g_1(x) \\ g_2(x) \end{bmatrix} \right\} \quad (41)$$

At this point, we develop algebra and further simplify it with (42) and (43).

$$G_1 = m_{11}^{-1} f_1 + m_{12}^{-1} f_2 \quad (42)$$

$$G_2 = m_{21}^{-1} f_1 + m_{22}^{-1} f_2 \quad (43)$$

As with the single link system, the fractional order approximation (44) is applied, and a program similar to the 1 DOF robot is used to finally obtain the fractional order model shown in (45).

$$\begin{bmatrix} s^\mu x_1 \\ s^\mu x_2 \\ s^\mu x_3 \\ s^\mu x_4 \end{bmatrix} = \begin{bmatrix} x_2 \\ G_1 \\ x_4 \\ G_2 \end{bmatrix}$$

(44)

In (44), the approximation shown in (12) is performed, and algebra and simplification terms are performed. Finally, the fractional order model of 2 DOF robot is established.

$$\begin{bmatrix} x_1 \\ x_2 \\ x_3 \\ x_4 \end{bmatrix} = \begin{bmatrix} \left(\dfrac{T}{A^2}\right)\dot{G}_1 + \dfrac{T}{A}G_1 + T\left(\dfrac{A^2-1}{A^2}\right)x_{2t} + x_{1t}\left(1-\dfrac{T}{A}\right) \\ \left(\dfrac{T}{A}\right)\dot{G}_1 + TG_1 + x_{2t}\left(1-\dfrac{T}{A}\right) \\ A_2 + \dfrac{T}{A}G_2 + T\left(\dfrac{A^2-1}{A^2}\right)x_{4t} + x_{3t}\left(1-\dfrac{T}{A}\right) \\ \left(\dfrac{T}{A}\right)\dot{G}_2 + TG_2 + x_{4t}\left(1-\dfrac{T}{A}\right) \end{bmatrix}$$

(45)

In (45), I = 1 $i = 2$ until.

$$\dot{G}_i \approx \frac{G_i(t-T) - G_i(t-2T)}{T}$$

(46)

Arrangements similar to (18) could have been proposed, but in this case $(A_{11}, A_{12}, A_{21}, A_{22})$ would be a matrix.

Finally, the fractional order model of 3 DOF robot is given, and its modeling scheme is shown in the **Figure 4**. The 3 DOF robot model in the reference dose not meet the requirements in **Figure 4.** Therefore, the modeling is carried out step by step from direct kinematics, inverse kinematics and Euler-Lagrange, and the calculation is repeated to check the error. Once the correct equation is obtained, the parameters given in **Table 4** are applied.

For 3 DOF robot, the Euler-Lagrange model shown in (47) is taken as the starting point.

$$\begin{bmatrix} \ddot{q}_1 \\ \ddot{q}_2 \\ \ddot{q}_3 \end{bmatrix} = \begin{bmatrix} i_{11} & i_{12} & i_{13} \\ i_{21} & i_{22} & i_{23} \\ i_{31} & i_{32} & i_{33} \end{bmatrix}\left\{\begin{bmatrix} \tau_1 \\ \tau_2 \\ \tau_3 \end{bmatrix} - \begin{bmatrix} c_{11} & c_{12} & c_{13} \\ c_{21} & c_{22} & c_{23} \\ c_{31} & c_{32} & c_{33} \end{bmatrix}\begin{bmatrix} \dot{q}_1 \\ \dot{q}_2 \\ \dot{q}_3 \end{bmatrix} - \begin{bmatrix} b_1\dot{q}_1 \\ b_2\dot{q}_2 \\ b_3\dot{q}_3 \end{bmatrix} - \begin{bmatrix} g_1 \\ g_2 \\ g_3 \end{bmatrix}\right\}$$

(47)

In equation (47), the inverse matrix I is (48):

$$\begin{bmatrix} i_{11} & i_{12} & i_{13} \\ i_{21} & i_{22} & i_{23} \\ i_{31} & i_{32} & i_{33} \end{bmatrix} = \begin{bmatrix} m_{11} & m_{12} & m_{13} \\ m_{21} & m_{22} & m_{23} \\ m_{31} & m_{32} & m_{33} \end{bmatrix}^{-1}$$

$$= \frac{1}{\Delta}\begin{bmatrix} m_{22}m_{33} - m_{23}m_{32} & m_{13}m_{32} - m_{12}m_{33} & m_{12}m_{23} - m_{13}m_{22} \\ m_{23}m_{31} - m_{21}m_{33} & m_{11}m_{33} - m_{13}m_{31} & m_{13}m_{21} - m_{11}m_{23} \\ m_{21}m_{32} - m_{22}m_{31} & m_{12}m_{31} - m_{11}m_{32} & m_{11}m_{22} - m_{12}m_{21} \end{bmatrix}$$

(48)

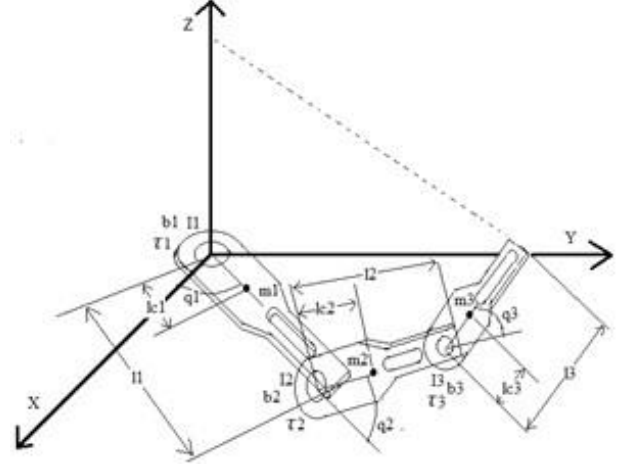**Figure 4.** Schematic diagram of three degree of freedom robot.

As determinant (49):

$$\Delta = m_{11}\left(m_{22}m_{33} - m_{23}m_{32}\right) + m_{12}\left(m_{23}m_{31} - m_{21}m_{33}\right) +$$

$$+ m_{13}\left(m_{21}m_{32} - m_{22}m_{31}\right)$$

(49)

From (50) to (67), each element of the matrix is represented by physical parameters. Due to the symmetry of the *M* matrix, some terms of the matrix are equal, as shown in (51), (52) and (54).

$$m_{11} = m_1 ll_1^2 + I_1 + m_2 l_1^2 + 2m_3 l_1 l_2 \cos(q_2) + m_2 l_2^2 \cos^2(q_2) + I_2 + m_3 l_1^2$$
$$+ 2m_3 l_1 l_2 \cos(q_2) + 2m_3 l_1 lc_3 \cos(q_2 + q_3) + m_3 l_2^2 \cos^2(q_2)$$

$$+ 2m_3 l_2 lc_3 \cos(q_2)\cos(q_2 + q_3) + m_3 lc_3^2 \cos^2(q_2 + q_3) + I_3$$

(50)

$$m_{12} = m_{21} = I_2 + I_3$$

(51)

$$m_{13} = m_{31} = I_3$$

(52)

$$m_{22} = m_2 lc_2^2 + m_3 l_2^2 + m_3 lc_1^2 + I_2 + I_3 + 2m_3 l_2 lc_3 \cos(q_3)$$

(53)

$$m_{23} = m_{32} = I_3 + m_3 l l_2 l c_3 \cos(q_3) + m_3 l c_3^2 \tag{54}$$

$$m_{33} = I_3 + m_3 l c_3^2 \tag{55}$$

Table 4. Physical parameters of three degree of freedom manipulator

Parameter	Link 1	Link 2	Link 3	Unit
Quality	m_1	m_2	m_3	kg
	19.5	1.3	1.1	
Length	L_1	L_2	L_3	m
	1.2	1.1	1.1	
Centroid length	lc_1	lc_2	lc_3	m
	0.5	0.5	0.5	
Moment of inertia	I_1	I_2	I_3	kg·m^2
	4.15	0.37	0.271	
Viscous friction coefficient	b1	b2	b3	N·m·s^{-1}
	1.8	1.8	1.8	
Torsion	τ1	τ2	τ3	N
Angular position	q_1	q_2	q_3	Grade
Angular velocity	$\dot{q}_1$	$\dot{q}_2$	$\dot{q}_3$	grade·s^{-1}
Accelerate angular	$\ddot{q}_1$	$\ddot{q}_2$	$\ddot{q}_3$	grade·s^{-2}

The Coriolis matrix of 3 DOF robot represents the dependence of angular position q2 and q3, and there is no equal term in this matrix.

$$c_{11} = -2m_2 l_1 l_2 \dot{q}_2 \, \text{sen}(q_2) - 2m_2 l_2^2 \dot{q}_2 \cos(q_2)\text{sen}(q_2)$$
$$-2m_3 l_1 l_2 \dot{q}_2 \, \text{sen}(q_2) - 2m_3 l_1 l c_3 \dot{q}_2 \, \text{sen}(q_2 + q_3) \tag{56}$$

$$c_{12} = -2m_3 l_2^2 \dot{q}_1 \cos(q_2)\text{sen}(q_2)$$
$$-2m_3 l_2 l c_3 q_1 \cos(q_2)\text{sen}(q_2 + q_3)$$
$$-2m_3 l c_3^2 \dot{q}_1 \cos(q_2 + q_3)\text{sen}(q_2 + q_3) \tag{57}$$

$$c_{13} = -2m_3 l_1 l c_3 \dot{q}_1 \, \text{sen}(q_2 + q_3)$$
$$-2m_3 l_2 l c_3 \dot{q}_1 \, \text{sen}(q_2 + q_3)\cos(q_2)$$
$$-2m_3 l c_3^2 \dot{q}_1 \cos(q_2 + q_3)\text{sen}(q_2 + q_3) \tag{58}$$

$$c_{21} = m_3 l_1 l_2 \dot{q}_1 \, \text{sen}(q_2) + \boldsymbol{m_3 l_1 l_3 \dot{q}_1 \, \mathbf{sen}(q_2 + q_3)}$$
$$+m_3 l_2^2 \dot{q}_1 \cos(q_2)\text{sen}(q_2) + 2m_3 l_2 l c_3 \dot{q}_1 \cos(q_2)\text{sen}(q_2 + q_3)$$
$$+2m_3 l_2 l c_3 \dot{q}_1 \, \text{sen}(q_2)\cos(q_2 + q_3)$$
$$+2m_3 l_3^2 \dot{q}_1 \cos(q_2 + q_3)\text{sen}(q_2 + q_3) \tag{59}$$

$$c_{22} = -2m_3 l_2 l c_3 \dot{q}_3 \, \text{sen}(q_3) \tag{60}$$

$$c_{23} = -m_3 l_2 l c_3 \dot{q}_3 \, \text{sen}(q_3) \tag{61}$$

$$c_{31} = m_3 l_1 l c_3 \dot{q}_1 \, \text{sen}(q_2 + q_3)$$
$$+ m_3 l_2 l c_3 \dot{q}_1 \cos(q_2)\text{sen}(q_2 + q_3)$$
$$+ m_3 l c_3^{22} q_1 \cos(q_2 + q_3)\text{sen}(q_2 + q_3) \tag{62}$$

$$c_{32} = -m_3 l_2 l c_3 \dot{q}_3 \, \text{sen}(q_3) \tag{63}$$

$$c_{33} = m_3 l_2 l c_3 \dot{q}_2 \, \text{sen}(q_3) \tag{64}$$

The terms related to gravity are given in sections 2 and 3. In section 1, since gravity is parallel to the earth's surface, there is no dependence on gravity.

$$g_1 = 0 \tag{65}$$

$$g_2 = m_2 g l c_2 \cos(q_2) + m_3 g l_2 \cos(q_2) + m_3 g l c_3 \cos(q_2 + q_3) \tag{66}$$

$$g_3 = m_3 g l c_3 \cos(q_2 + q_3) \tag{67}$$

Using the same method for 1 and 2 DOF system, the fractional dynamic model of 3 DOF robot is (68):

$$\begin{bmatrix} x_1 \\ x_2 \\ x_3 \\ x_4 \\ x_5 \\ x_6 \end{bmatrix} = \begin{bmatrix} \left(\dfrac{T}{A^2}\right)\dot{G}_1 + \dfrac{T}{A}G_1 + T\left(\dfrac{A^2-1}{A^2}\right)x_{4t} + x_{1t}\left(1-\dfrac{T}{A}\right) \\ \left(\dfrac{T}{A^2}\right)\dot{G}_2 + \dfrac{T}{A}G_2 + T\left(\dfrac{A^2-1}{A^2}\right)x_{5t} + x_{2t}\left(1-\dfrac{T}{A}\right) \\ \left(\dfrac{T}{A^2}\right)\dot{G}_3 + \dfrac{T}{A}G_3 + T\left(\dfrac{A^2-1}{A^2}\right)x_{6t} + x_{3t}\left(1-\dfrac{T}{A}\right) \\ \left(\dfrac{T}{A}\right)G_1 + TG_1 + x_{4t}\left(1-\dfrac{T}{A}\right) \\ \left(\dfrac{T}{A}\right)\dot{G}_2 + TG_2 + x_{5t}\left(1-\dfrac{T}{A}\right) \\ \left(\dfrac{T}{A}\right)\dot{G}_3 + TG_3 + x_{6t}\left(1-\dfrac{T}{A}\right) \end{bmatrix}$$

(68)

(68) applies to (69) and (70):

$$\begin{vmatrix} G_1 \\ G_2 \\ G_3 \end{vmatrix} = \begin{vmatrix} i_{11} & i_{12} & i_{13} \\ i_{21} & i_{22} & i_{23} \\ i_{31} & i_{32} & i_{33} \end{vmatrix}$$

$$\left\{ \begin{bmatrix} kp_1(q_{d1}-q_1) - kv_1\dot{q}_1 - c_{11}\dot{q}_1 - c_{12}\dot{q}_2 - c_{13}\dot{q}_3 - b_1\dot{q}_1 \\ kp_1(q_{d2}-q_2) - kv_2\dot{q}_2 - c_{21}\dot{q}_1 - c_{22}\dot{q}_2 - c_{23}\dot{q}_3 - b_2\dot{q}_2 \\ kp_1(q_{d3}-q_3) - kv_3\dot{q}_3 - c_{31}\dot{q}_1 - c_{32}\dot{q}_2 - c_{33}\dot{q}_3 - b_3\dot{q}_3 \end{bmatrix} \right\}$$

(69)

$$\begin{bmatrix} \dot{G}_1 \\ \dot{G}_2 \\ \dot{G}_3 \end{bmatrix} \approx \begin{bmatrix} \dfrac{G_1 - G_{1\_t}}{T} \\ \dfrac{G_2 - G_{2\_t}}{T} \\ \dfrac{G_3 - G_{3\_t}}{T} \end{bmatrix}$$

(70)

3. Result

This section compares the integer order model with the model developed using FOC. **Figure 5** shows the response diagram of the first-order integer and second-order fractional robot connecting rod, and the order of the fractional derivative is $\mu = 0.99$ and $\mu = 0.95$. The very similar diagram shows that the steady-state error is more obvious for the fractional order model. If the value of μ is small, this is what we want to prove. The velocity diagram of link 1 also shows that the velocity approaches zero, i.e. the equilibrium value is reached. As shown in the **Figure 5**, the fractional order response is slower than the integer order model. In fact, if the fractional order model with high response speed is to be simulated, the continuous fractional approximation (8) must have more terms. The more terms, the more accurate the bandwidth of the fractional order model[9]. Finally, in this simulation, the q_1 required angle is 90° .
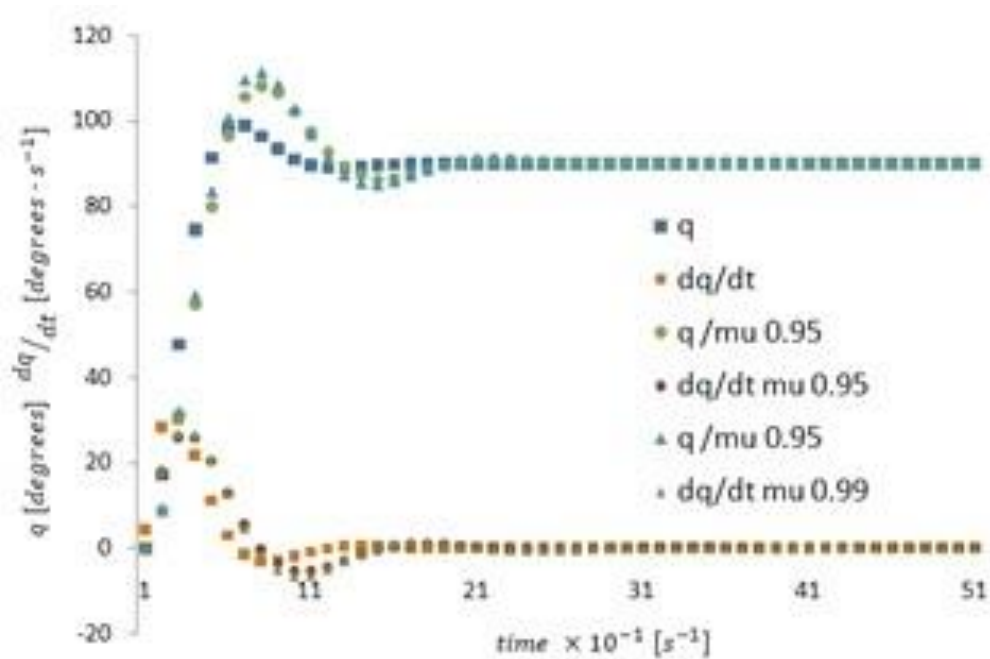

Figure 5. Graphical response of the 1 DOF robot.

Figure 6 shows the response diagram of connecting rod 1 of the 2 DOF robot, which is of integer order and two fractional orders, and the order of the fractional derivative is $\mu = 0.99$ and $\mu = 0.95$. The fractional order diagram shows that the error in the steady state is easier to observe, and the speed approaches zero, i.e. it reaches the equilibrium value. In the simulation, the q_1 and q_2 required angle is 10°.
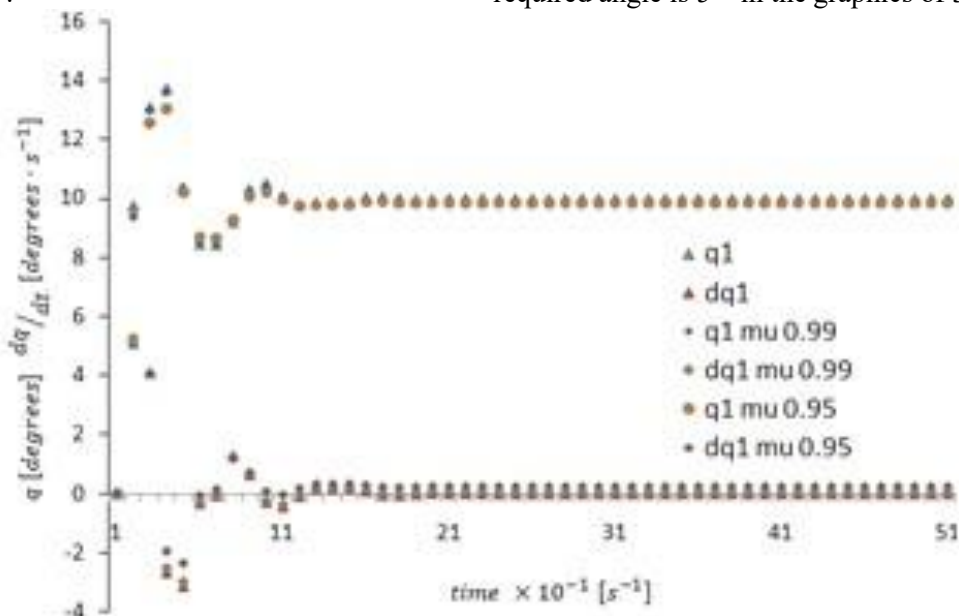
Figure 7 shows the response diagram of the connecting rod 1 of the 3 DOF robot, which is of integer order and two fractional orders, and the fractional derivative is $\mu = 0.99$ and $\mu = 0.95$. The fractional order diagram shows that the error in the steady state is easier to observe, and the speed approaches zero, i.e. it reaches the equilibrium value. In the simulation, the q_1, q_2 and q_3 required angle is 5° in the graphics of 3 DOF robot.
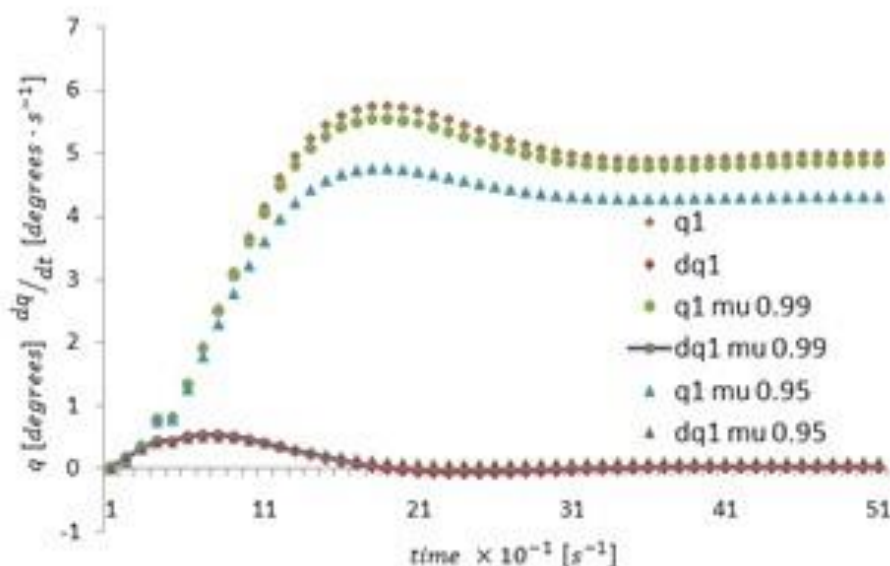

Figure 6. Response diagram of connecting rod 1 of the 2 DOF robot.

Figure 7. Response diagram of connecting rod 1 of the 3 DOF robot.
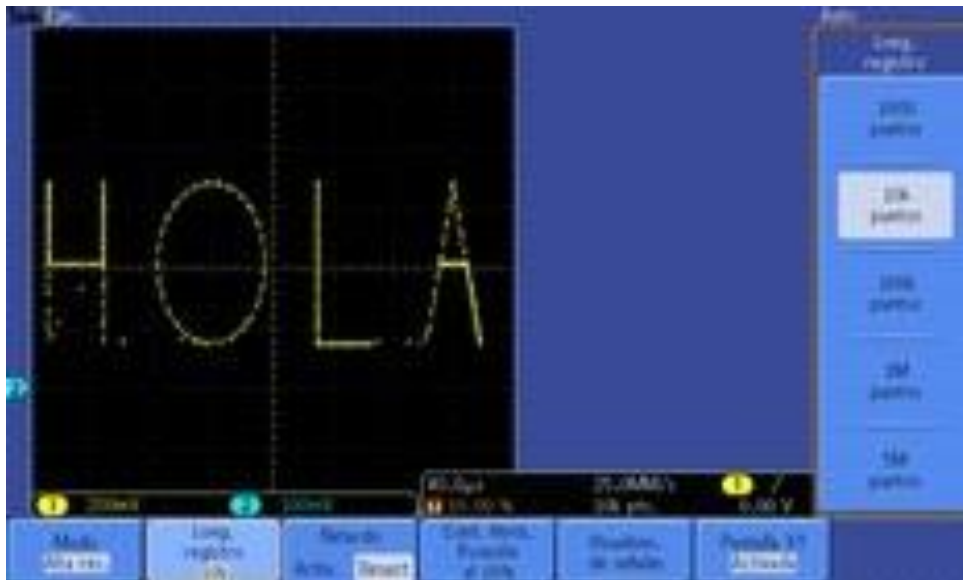
Figure 8. Output the image of "HOLA" track on the oscilloscope.

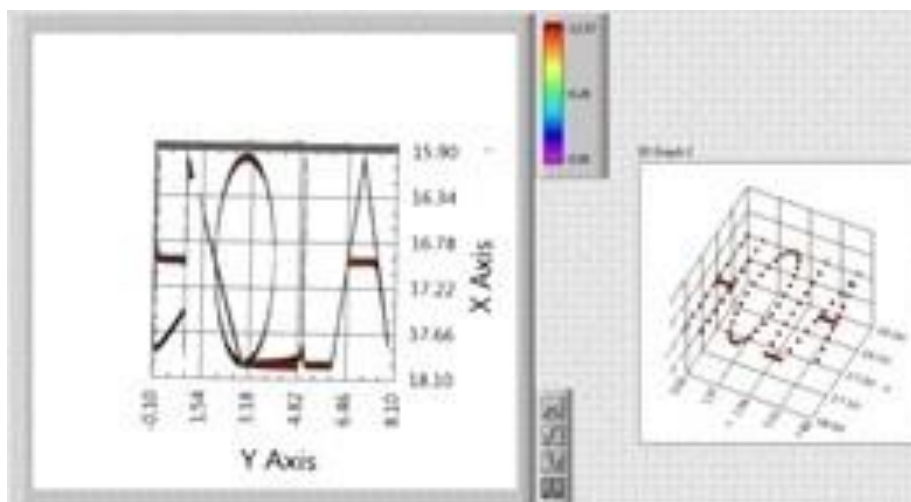**Figure 9.** The figure shows the "HOLA Dr CHUA" track output by the oscilloscope.

Figure 10. Set the "HOLA" path for the score model of 3 DOF in LabVIEW.

Within the application scope of these models, the trajectories of 2 and 3 DOF models and "H" "O" "L" "A" are designed by using the advantages of STM32L476 card. In the case of 2 DOF model, the route is drawn by oscilloscope, as shown in the **Figure 8**. In addition, a path of "HOLA Dr CHUA" is designed and displayed on the oscilloscope. For the 3 DOF model, the "HOLA " track is drawn in LabVIEW, as shown in **Figure 10**.

Figures 8 and **9** are obtained using Tektronix DPO3032 oscilloscope. Photos of greetings to the head of ITSPR are shown in the **Figure 9**.

4. Conclusion

The results show that the fractional order modeling of the dynamic model of the rotating manipulator will produce convergence results when it is expected to reach a certain position or describe a trajectory in the point-to-point control method. In fact, the fractional order must be close to the first order, which shows that the difference between the traditional integer order model and the fractional order model is not significant. The fractional order model includes the following points.

1. The results show that the fractional order dynamic model meets the second criterion of Lyapunov stability, which shows that the model has convergence.

2. The simulation diagram shows the expected error of the fractional order model in the steady state, which means that the fractional order model is more accurate than the integer order model.

3. The fractional order model allows to simulate the complex trajectories of 2 and 3 DOF systems, which are implemented on STM32L476 development card and displayed on oscilloscope.

Conflict of interest

None declared./The authors declare that they have no conflict of interest.

Acknowledgement

References

1. Goméz-Aguilar JF, Rosales-García J, Razo-Hernández JR., et al. Fractional RC and LC electrical circuits. Ingeniería, Investigación y Tecnología 2014; 15(2): 311–319.

2. Goodvine B, Leyden K. Recent results in fractional order modeling in multi-agent systems and linear friction welding. IFAC-PapersOnLine 2015; Vol. 48(1): 380–381.

3. Tejado I, Valerio D, Pires P, et al. Fractional human arm dynamics with variability analyses. Mechatronics 2013; 23(7): 805–812.

4. Rosario JM, Dumur D, Tenreiro M. Analysis of fractional-order robot axis dynamics. IFAC Proceedings Volumes 2006; 39(11): 367–372.

5. Shalaby R, El-Hossaing M, Abo-Zalam B. Fractional Order modeling and control for under-actuated inverted pendulum. Communications in Nonlinear Science and Numerical Simulation 2019; 74: 97–121.

6. Zhang L, Hu X, Wang Z, et al. Fractional-Order modeling and State-of-Charge estimation for ultracapacitors. Journal of Power Sources 2016; 314: 28–34.

7. Shi X, Chen YQ, Huang J. Application of fractional-order active disturbance rejection controller on linear motion system. Control Engineering Practice 2018; 81: 207–214.

8. Ceron-Morales I, Gonzalez-Manzanilla FQ, Muñiz-Montero C, et al. Control PID de orden fraccional aplicado a un colector solar cilindroparabólico [Application of Fractional Order PID control in solar collector]. Visión Politécnica 2018; 13(1): 23–27.

9. Krishna BT. Studies on fractional differentiators and integrators: A survey. Signal Processing 2011; 91(3), 246–386.

10. Sun H, Zhang Y, Dumitru B, et al. A new collection of real world practical applications of fractional calculus in science and engineering. Communication in Nonlinear Science and Numerical Simulations 2018; 64: 213–231.

11. Muñiz-Montero C, Flores JA, Ceron I, et al. Implementación de controladores PID fraccionales en las plataformas STM32-Discovery y Arduino a partir de SIMULINK/MATLAB: Parte I [Implementation of Fractional Order PID controller based on Simulink / Matlab STM32 discovery and Arduino platform: Part I]. Visión Politécnica 2017; 12(2): 8–12.

12. Ceron-Morales I, Muñiz-Montero C, Tlelo-Cuautle E. Metodología didáctica de control con redes neuronales y FOPID al modelo dinámico de un robot 2GDL en Arduino y STM32. XVII Congreso Nacional de Ingeniería

Electromecánica y de Sistemas; 2018; Mexico City. 2018.

13. Cero I, Herver Acuña JF, Castillo-Castillo SJ, et al. Metodología de programación de trayectorias de un robot de 2GDL Utilizando la tarjeta STM32L476RG [Methodology for programming 2DOF robot trajectory using STM32L476RG card]. In: Sinergia Mecatrónica. Asociación Mexicana de Mecatrónica A.C.; 2019. p. 144–158.

14. Voronin BF. La aplicación del método de fragmentación en la enseñanza de cinemática de mecanismos [Application of segmented kinematics in the teaching of science]. Científica 2014; 18(1): 21–29.

15. Zhang D, Wei B. A review on model reference adaptive control of robotic manipulators. Annual Reviews in Control 2017; 43: 188–198.

16. Ramirez-Agundis A, Orozco-Mendoza H, Villaseñor-Aguilar M. Control de estabilidad de un manipulador planar paralelo 3RRR utilizando redes neuronales [stability of planar 3RRR parallel robot controlled by neural network] Científica 2011; 15(3): 107–115.